Clim Dyn (2017) 48:3599–3614
DOI 10.1007/s00382-016-3287-0

The response of winter Pacific North American pattern to strong volcanic eruptions

Zhongfang Liu[1] · Kei Yoshimura[2] · Nikolaus H. Buenning[3] · Zhimin Jian[1] · Liang Zhao[4]

Received: 1 February 2016 / Accepted: 18 July 2016 / Published online: 26 July 2016

Abstract The impact of volcanic eruptions on large-scale atmospheric circulation patterns has been well studied, but very little effort has been made on relating the response of Pacific North American (PNA) pattern to strong volcanic eruptions. Here we investigate the response of winter PNA to the largest volcanic eruptions using three different reanalysis datasets. We demonstrate a significant positive PNA circulation response to strong volcanic forcing in the first winter following the eruptions. This circulation pattern is associated with enhanced southwesterly winds advecting warm air from the tropical/subtropical Pacific into northwestern North America and leads to a significant warming in the region. However, no significant PNA signal is found for the second post-eruption winter. The PNA responses to volcanic forcing depend partly upon the modulation of the El Niño Southern Oscillation (ENSO) events. When the ENSO influence is linearly removed, this positive PNA signal is still robust during the first post-eruption winter, albeit with slightly decreased magnitude and significance. Our findings provide new evidence for volcanic forcing of the Pacific and North American climates. The results presented here may contribute to deconvolving modern and past continental-scale climate changes over North America.

Keywords PNA · ENSO · Volcanic eruptions · Superposed epoch analysis

1 Introduction

Empirical evidence from the Northern Hemisphere (Briffa et al. 1998; Mann et al. 2012; Esper et al. 2013) and results from climate simulations (Stenchikov et al. 2002, 2006; Iles et al. 2013) have indicated that strong explosive volcanic eruptions can exert an important influence on the global climate on many timescales through radiative, chemical, dynamic and thermal processes (Robock 2000). Particularly, land surface temperatures during boreal winter have significantly increased during the 2 years after strong volcanic eruptions in regions of Northern Europe, Russia and northwestern North America (Robock and Mao 1992, 1995; Shindell and Schmidt 2004; Fischer et al. 2007). This temperature response also holds true when the influence of the El Niño Southern Oscillation (ENSO) is removed (Robock and Mao 1992, 1995). The processes responsible for the warming over Northern Europe and Russia have been argued to be a result of a volcano-induced positive phase of the North Atlantic Oscillation (NAO)/Arctic Oscillation (AO), which enhances the zonal winds bringing warm maritime air from the North Atlantic to the continent (Kodera 1994; Perlwitz and Graf 1995). On the other hand, the winter warming over northwestern North America after strong eruptions is probably related to a change to a more positive phase of the Pacific-North American (PNA) circulation pattern that substantially increases the southwesterly flows into the northwestern regions of the continent (Perlwitz and Graf 1995).

Electronic supplementary material The online version of this article (doi:10.1007/s00382-016-3287-0) contains supplementary material, which is available to authorized users.

✉ Zhongfang Liu
liuzf406@gmail.com

[1] State Key Laboratory of Marine Geology, Tongji University, Shanghai, China

[2] Atmosphere and Ocean Research Institute, University of Tokyo, Kashiwa, Japan

[3] Department of Earth Sciences, University of Southern California, Los Angeles, CA, USA

[4] 61741 Troops, Beijing, China

Given the importance of extratropical circulations in connecting surface climates with volcanic eruptions, much effort has been devoted to investigating the atmospheric circulation responses to strong volcanic forcing. So far, the main focus of circulation/volcanic forcing research has centered on the effects of major eruptions on the NAO/AO, which suggests a pronounced positive phase of the NAO/AO in the Atlantic sector during the two winters following a major eruption (Stenchikov et al. 2002, 2006; Christiansen 2008). Some studies have also explored the response of the Southern Hemisphere annular mode (SAM) to strong volcanic eruptions and found a weak link between volcanic eruptions and SAM in the following two austral winters (Robock et al. 2007). However, very little work has been done relating the PNA response to volcanic forcing. Analysis of monthly historical mean sea level pressure (MSLP) data indicates a significant positive phase of the PNA pattern in the first post-eruption winter (Christiansen 2008). An investigation based on results from the comprehensive Earth system model developed at the Max Planck Institute for Meteorology (MPI-ESM) further revealed that the 500-hPa geopotential heights display an anomalous structure resembling the positive phase of the PNA during the first two winters following an eruption, but tend thereafter toward a negative phase of the PNA over the next decade (Zanchettin et al. 2012, 2013). Despite these efforts and the acquired fundamental knowledge about the PNA responses to the volcanic forcing, there are still some uncertainties due to the short records of atmospheric data, timeframe, and the number of eruptions or model realizations. Moreover, the effects of eruption on the PNA may be confounded by other sources of variability such as ENSO events (Christiansen 2008), especially for the near-simultaneous occurrence of El Niño events that tend toward a positive phase of the PNA (Renwick and Wallace 1996; Yu et al. 2007). Thus, a more rigorous examination of the mid-tropospheric geopotential heights is necessary to evaluate the PNA response to the volcanic eruptions, especially considering the possible influence of the ENSO on the PNA.

Although climate models can provide a more rigorous test of how the largest volcanic eruptions affect climate variability (Kirchner et al. 1999; Stenchikov et al. 2002; Timmreck 2012), analysis of the current state-of-the-art Coupled Model Intercomparison Project 5 (CMIP5) models shows a large spread in simulating the observed dynamical response to strong volcanic eruptions (Driscoll et al. 2012; Charlton-Perez et al. 2013). Hence, in this study, we use three different reanalysis data sets to investigate the responses of the PNA to the six largest volcanic eruptions in either the Northern Hemisphere or the tropics (Table 1; Fig. 1a). To this end, composite anomaly maps of surface temperature, MSLP, and 500-hPa geopotential height fields for the first and second winters after the eruptions are constructed to explore common circulation patterns associated with the eruptions. We then compute time series of winter temperature anomalies and PNA indices for different reanalysis data sets and use a superposed epoch analysis (SEA) (Mitchell 1961; Adams et al. 2003) to quantify the change to the PNA following these large eruptions. Considering the possible modulation of ENSO on surface temperature anomalies and the PNA, we repeat the above analysis with the ENSO signal removed. Finally, we present a discussion of the possible mechanisms for the PNA response to volcanic eruptions and implications of our results for the detection and attribution of modern and past climatic changes in North America.

Table 1 List of the 6 largest volcanic eruptions used in this study, which is taken from Iles et al. (2013), with the volcanic aerosol optical depth (AOD) at 550 nm greater than 0.05 (Sato et al. 1993)

Volcano	Eruption date	Latitude	Winters analyzed	Reference period
Krakatau	August 1883	6°S	1883–1884, 1884–1885	1874–1883
Santa Maria	October 1902	13°N	1903–1904, 1904–1905	1894–1903*
Novarupta	June 1912	58°N	1912–1913, 1913–1914	1906–1912
Agung	March 1963	8°S	1963–1964, 1964–1965	1954–1963
El Chichón	April 1982	17°N	1982–1983, 1983–1984	1973–1982
Pinatubo	June 1991	15°N	1991–1992, 1992–1993	1985–1991

The reference period marked with * is 1901–1903 for the ERA-20C dataset

2 Data

We used monthly surface temperature, MSLP and 500-hPa geopotential height data taken from three reanalysis datasets: the Twentieth Century Reanalysis version 2 (20CRv2; Compo et al. 2011), the ERA Twentieth Century (ERA-20C; Poli et al. 2013) and the National Centers for Environmental Protection-National Center for Atmospheric Research reanalysis 1 (NCEP/NCAR R1; Kalnay et al. 1996). The 20CRv2 is a global atmospheric circulation dataset based on observational constraints from 1871 to 2012 on a $2° \times 2°$ global grid. This dataset includes a 56-member filtered ensemble that provides atmospheric fields and uncertainties every 6 hours. The ERA-20C reanalysis provided by the European Centre for Medium-Range Weather Forecasts (ECMWF) is a 10-member reanalysis of the twentieth century (1900–2010), assimilating surface observations from the International Comprehensive Ocean–Atmosphere Data

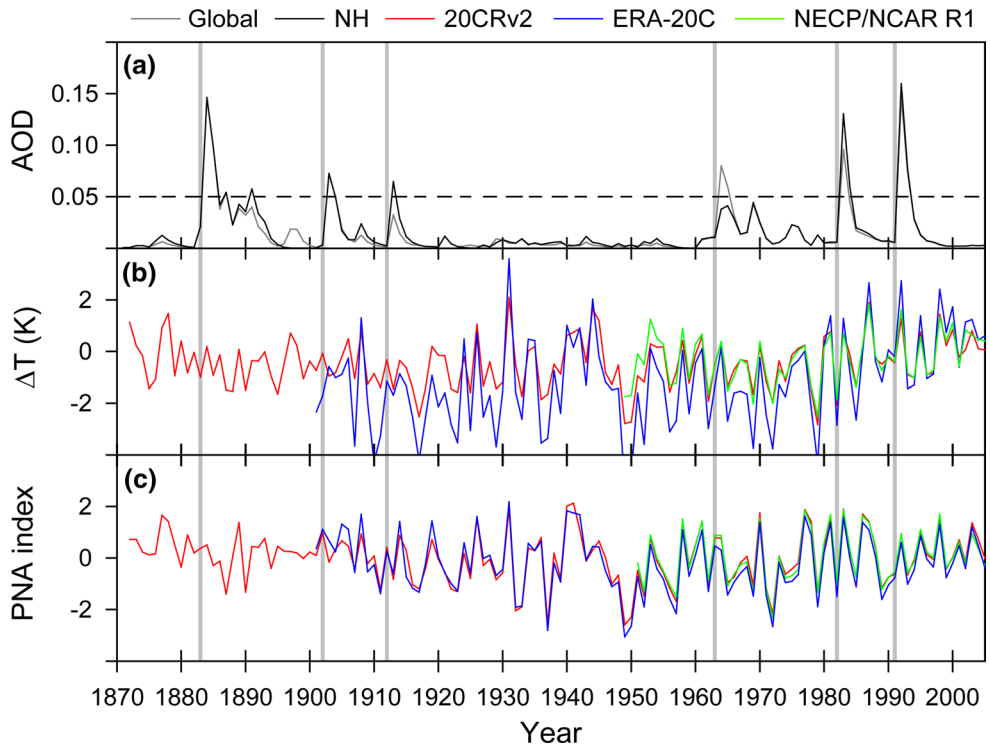

Fig. 1 **a** Winter (DJF) average volcanic aerosol optical depth (AOD) at 550 nm for the global and North Hemisphere based on Sato et al. (1993). **b** Surface temperature anomaly (ΔT; K) averaged over the northwestern North America (130°W–90°W, 40°N–60°N). **c** PNA index based on the 20CRv2, the ERA-20C and the NCEP/NCAR R1, respectively. The ΔT and PNA index are calculated as the departures from the 1980–2000 base-period mean. *Black dashed line* denotes the 0.05 AOD cutoff used for selecting the six eruptions, as showed by *vertical grey lines*

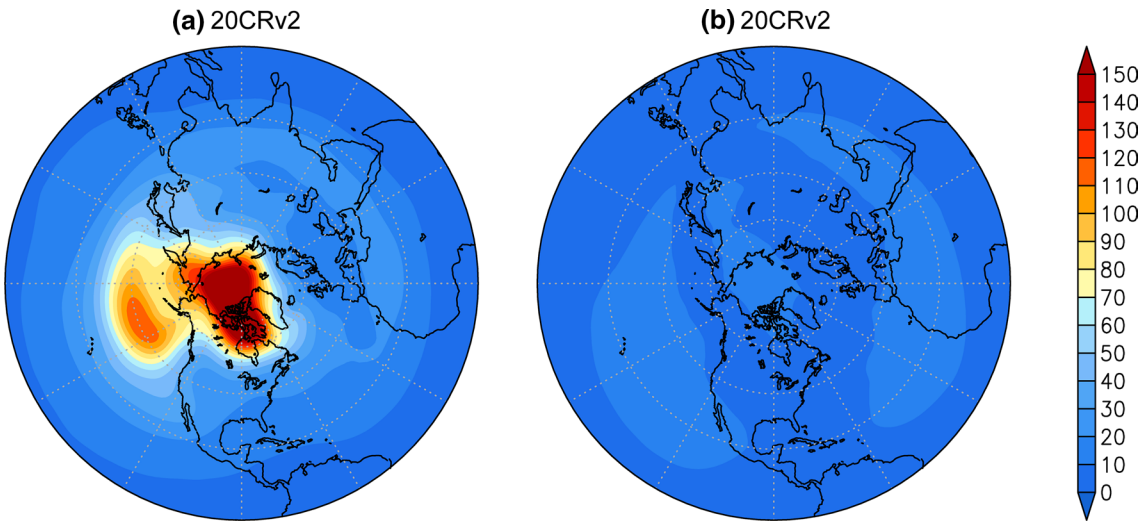

Fig. 2 The ensemble spread (m) of winter averages for the 20CRv2 500-hPa geopotential height for **a** the first three volcanic winters (1883/1884, 1903/1904 and 1912/1913) and **b** recent three volcanic winters (1963/1964, 1982/1983 and 1991/1992)

Set (ICOADS), with a spatial resolution of 1.125° × 1.125°. For both twentieth century reanalysis datasets, the ensemble mean fields are used for our analysis. Both reanalyses are subject to higher uncertainty in the early decades due to fewer assimilated observational data (Compo et al. 2011; Poli et al. 2013). For example, the 20CRv2 shows large ensemble spread (standard deviation) in 500-hPa geopotential height over the North Pacific during the first three volcanic winters (1883/1984, 1903/1904 and 1912/1913) compared to recent three volcanic winters (1963/1964, 1982/1983 and 1991/1992) (Fig. 2). Similar uncertainty in this region holds true also for the earlier years of the ERA-20C (Poli et al. 2013), though the ensemble members or ensemble spread are not yet available. Despite high uncertainty before 1950, the calculated PNA indices based on two reanalysis datasets show good consistency in magnitude and time evolution (Fig. 1c). For comparison, the same climate fields from the NCEP/NCAR R1 (1948–2015) are also used.

In contrast to above two twentieth century reanalyses that are based only on surface observations, the NCEP/NCAR R1 also assimilates satellite and upper air data every 6 h, and is one of the most widely used reanalysis data sets. We calculate winter means of surface temperature, MSLP, and 500-hPa geopotential height fields by averaging the monthly means of December through February (DJF), obtaining 141, 110 and 67 complete winters for the 20CRv2, the ERA-20C and the NCEP/NCAR R1, respectively.

To quantify ENSO variability we use the cold tongue index (CTI) (Deser and Wallace 1987), defined as the difference between sea surface temperature (SST) anomalies averaged over the region 6°N–6°S and 180°–90°W and the global-mean SST anomaly (available at http://jisao.washington.edu/enso). Winter means of the CTI from 1872 to 2005 are used in this study. Unless otherwise stated, all calculations are based on winter means.

3 Methods

3.1 Selection of volcanic events

The selection of the volcanoes can strongly affect the statistical analysis. Because the effect of volcanic eruptions on climate is most directly related to the aerosol radiative forcing in the stratosphere (Robock 2000), we follow Iles et al. (2013) and chose eruptions with global or North Hemisphere winter mean aerosol optical depths (AOD) above 0.05 (Sato et al. 1993) for our analysis. Based on this criterion, six strongest eruptions are selected during the 1871–2012 period covered by the 20CRv2 dataset. Table 1 lists these six volcanic eruptions and the winter periods analyzed for each eruption. To isolate the anomalies of the post-volcanic winters, we follow Stenchikov et al. (2006) and chose a different reference period (Table 1) for each eruption, then composites of the anomalies are calculated for the climate fields of interest for each reanalysis data set.

3.2 PNA index

To measure the strength of the PNA, winter PNA indices for the 20CRv2, the ERA-20C and the NCEP/NCAR R1 are constructed according to a modified point-wise method developed by the Climate Prediction Center (CPC 2016):

$$\begin{aligned}\mathrm{PNA} = {} & Z^{*}\left(15^{\circ}\mathrm{N}{-}25^{\circ}\mathrm{N}, 180^{\circ}{-}140^{\circ}\mathrm{W}\right) \\ & - Z^{*}\left(40^{\circ}\mathrm{N}{-}50^{\circ}\mathrm{N}, 180^{\circ}{-}140^{\circ}\mathrm{W}\right) \\ & + Z^{*}\left(45^{\circ}\mathrm{N}{-}60^{\circ}\mathrm{N}, 125^{\circ}\mathrm{W}{-}105^{\circ}\mathrm{W}\right) \\ & - Z^{*}\left(25^{\circ}\mathrm{N}{-}35^{\circ}\mathrm{N}, 90^{\circ}\mathrm{W}{-}70^{\circ}\mathrm{W}\right)\end{aligned} \quad (1)$$

where Z^{*} is the winter mean 500-hPa geopotential height anomaly that is computed as the departures from the 1980–2000 base-period means, and the (x) indicates spatial averaging over the domain x. All calculated winter PNA index time series are shown in Fig. 1, which indicates that the PNA indices derived from both the 20CRv2 and the ERA-20C are highly correlated each other ($r = 0.96$, 1901–2005 period), and both are also highly correlated with the NCEP/NCAR R1 ($r = 0.99$, 1951–2005 period).

3.3 Superposed epoch analysis

The superposed epoch analysis (SEA) has been widely used to investigate the effect of strong volcanic eruptions on climates (Mitchell 1961; Adams et al. 2003). We perform a SEA to determine the response of the PNA to each eruption listed in Table 1. To this end, we take the years of volcanic eruptions as "key dates". Given the key dates, we then sample the time series of surface temperature anomaly or PNA index using a window of data points centered on each key date. For each key date, a 7-year window is used in our analysis, with three data points on either side of the key date. The extracted windows are then averaged over the epochs. The SEA is performed on the time series of surface temperature anomalies and PNA indices for the three different reanalysis datasets. The statistical significance of the average temperature or PNA response to the eruptions is determined using a Monte Carlo-bootstrap approach, based on the null hypothesis that there is no association between the PNA (or temperature) and volcanic eruptions. Each volcanic event is randomly reassigned a new key date in the different periods (for the three different reanalysis datasets), respectively. The average PNA or temperature anomaly value is calculated for the key date and also the 6 years (−3 to +3) surrounding the key date (for 7 years in total). This process is repeated 1000 times to build a random distribution for the PNA or temperature anomaly values, against which the results of our SEA analyses are considered to be statistically significant at the 95 or 99 % confidence level when they are larger than 95 or 99 % of the Monte Carlo results.

3.4 Removing the ENSO influence

Previous studies have found that the positive phase of the PNA tends to occur during El Niño winters, and vice versa for La Niña winters (Renwick and Wallace 1996; Yu et al. 2007). Thus, the influence of volcanic eruptions on the PNA may be confounded by the simultaneous occurrence of ENSO events. Moreover, strong volcanic eruptions may be linked to an increase in El Niño events in the year following an eruption (Adams et al. 2003; Maher et al. 2015), albeit with some uncertainty (Mao and Robock 1998). Many previous studies have attempted to remove ENSO-associated variability in various ways (Compo and Sardeshmukh

2010, and references therein), but complete removal of ENSO influence is challenging due to the complexity of ENSO evolution. To minimize the influence of ENSO, we repeat our analysis by removing the ENSO signal from all analyzed winter climate fields (y) using a linear regression method (L'Heureux et al. 2013; Larson and Kirtman 2014):

$$y' = y - r(CTI, y) \times CTI \quad (2)$$

where y' is ENSO-independent winter climate fields; r is the regression coefficient of winter ENSO index (CTI) onto climate fields.

4 Results

4.1 Surface temperature response

Figure 3 shows the composite anomaly maps of surface temperature over North America during the first and second winters following the eruptions. A strong statistically significant ($p < 0.05$) warming (>1.5 K) is found over northwestern North America during the first post-eruption winter for all three reanalysis datasets (Fig. 3a, c e). This warming is consistent with previous findings (see Robock 2000) and demonstrates the robustness of this particular volcanic signal. Although the strength and homogeneity of this signal are slightly dependent upon the choice of volcanic eruptions, the positive temperature anomalies over northwestern North America are suggestive of a positive phase of the PNA (Fig. 4). The positive surface temperature anomalies during the first post-eruption winter show a narrow spatial extent compared to the positive correlations between the surface temperature and PNA index over northwestern North America, which suggests that not all eruptions can produce a positive PNA response during the first post-eruption winter (see Fig. 9). In contrast, all reanalyses do not show a warming in this region during the second post-eruption winter, but tend to exhibit a slight and insignificant cooling (Fig. 3b, d f). This is somewhat different from previous reports that expected a warming signal over northwestern North America during the second post-eruption winter (Robock and Mao 1992, 1995; Shindell and Schmidt 2004. 2004). Thus, our analysis reveals that average warming over northwestern North America during the two winters after the eruptions is mainly due to the first post-eruption winter, in which the positive PNA circulation leads to enhanced southwesterly winds (i.e., warm air advection) and positive temperature anomalies in the region.

4.2 Sea level pressure response

The surface expression of the PNA is the Aleutian low, which controls the shape of the mid-latitude jet stream and largely determines the PNA phase (Wallace and Gutzler 1981). The patterns of temperature anomalies associated with circulation changes are consistent with the MSLP anomalies (Fig. 5). For the first post-eruption winter, all reanalyses show a low pressure anomaly centered over the Aleutian Islands, albeit with very small significant ($p < 0.05$) areas (Fig. 5a, c, e). This negative MSLP anomaly over the Aleutian Islands depicts a slightly positive PNA pattern (Fig. 6), and are in agreement with results derived from the historical MSLP dataset (Christiansen 2008). The magnitude of this anomaly over the Aleutian Islands is approximately −2 hPa and more pronounced for the NCEP/NCAR R1 dataset that only covers the recent three eruptions. This negative MSLP anomaly is surrounded to the south by positive MSLP anomalies over the subtropical Pacific. The resulting meridional pressure gradient over the Pacific sector drives southwesterly flow into northwestern North America, which accounts for corresponding warm temperature anomalies in the region. In addition, the anomaly maps also reveal a positive NAO pattern in the north Atlantic sector for the first post-eruption winter (Fig. 5a, c, e). This positive NAO response over the North Atlantic is consistent with previous observational and modeling studies (Stenchikov et al. 2006; Christiansen 2008).

The second post-eruption winter is typically thought to have a similar but weaker climate response to volcanic forcing (Robock and Mao 1995; Christiansen 2008). Although the spatial patterns of the MSLP anomalies over the Atlantic sector depict a slightly positive NAO pattern during the second post-eruption winter (Fig. 5b, d, f), the expected positive PNA pattern is not found over the Pacific sector. Conversely, a slightly positive MSLP anomaly (1–3 hPa) around the Aleutian Islands is coupled with negative MSLP anomaly (>−2 hPa) over the subtropical Pacific, suggesting a slightly negative PNA signal. This circulation response to the volcanic eruptions is also consistent with surface temperature anomalies (Fig. 3b, d, f). Thus, the MSLP composites reveal that the PNA response to strong volcanic eruptions is only robust during the first post-eruption winter and tends to favor a positive phase the PNA.

4.3 Geopotential height response

Geopotential height anomalies in the mid- and upper-troposphere is typically used to measure the strength of the PNA (Wallace and Gutzler 1981). Figure 7 shows the composite anomaly maps of winter 500-hPa geopotential heights for the three reanalysis datasets. The composite anomalies show a quadrupolar structure in the Pacific and North American sectors during the first post-eruption winter, with centers of strong positive anomalies west of the Hawaii Islands and western North America (>10 m), and centers of strong negative anomalies over the Aleutian Islands

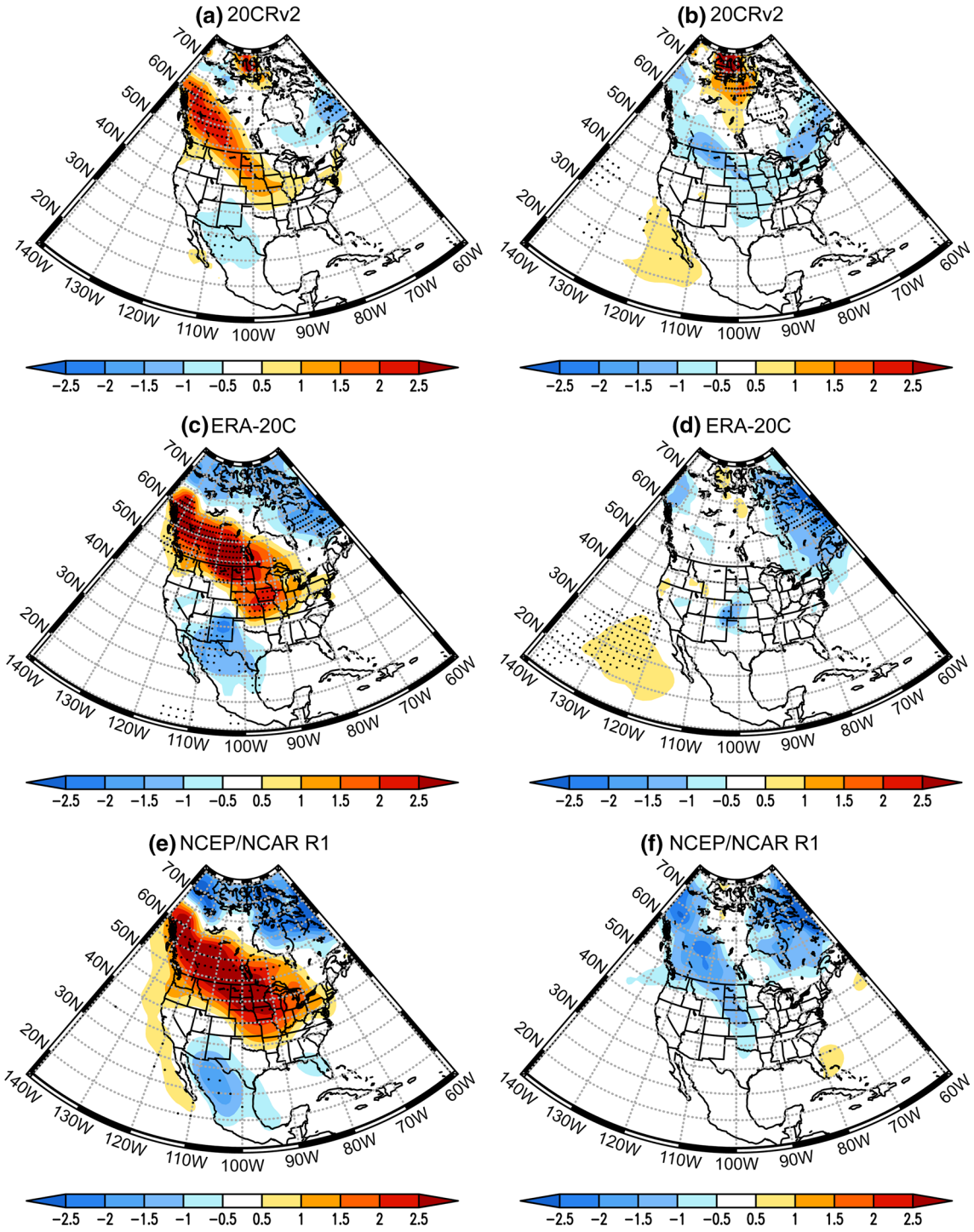

Fig. 3 Composite anomalies of the surface temperature (K) for the first (*left*) and second (*right*) winters following the eruptions based on the 20CRv2, the ERA-20C and the NCEP/NCAR R1, respectively. Areas with significance at the $p < 0.05$ level are stippled

(<−20 m) and southern United States (<−10 m) (Fig. 7a, c, e). Despite small areas of significance ($p < 0.05$), these anomaly centers (except the southeastern center which shifts west) are largely consistent with the four centers of action defined by the PNA (Wallace and Gutzler 1981), revealing a positive phase of the PNA (Fig. 8). The magnitude of the geopotential height anomalies is even stronger for the NCEP/NCAR R1 dataset. Despite differences in the strength and positioning of anomaly centers between the reanalysis datasets, the results suggest a more positive

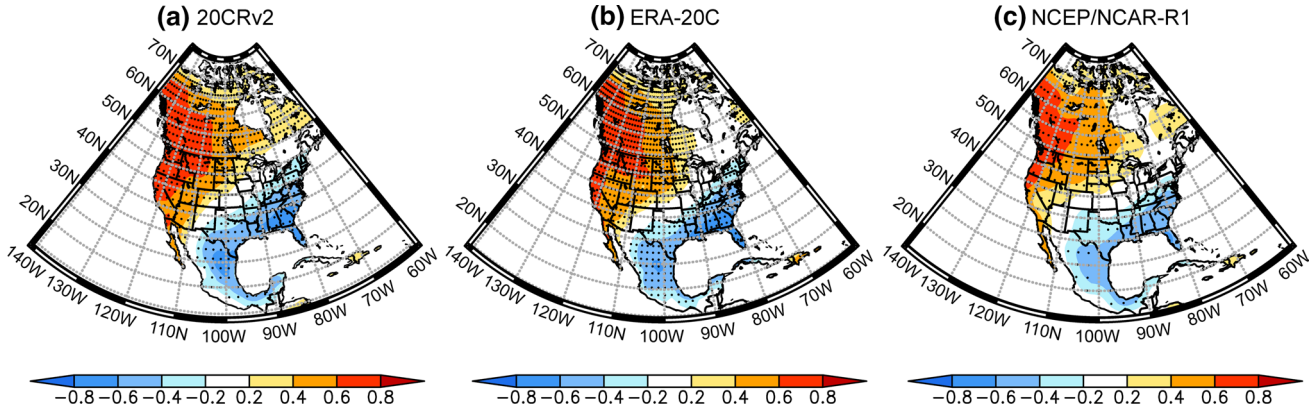

Fig. 4 Spatial correlations between the surface air temperature and the PNA index for **a** the 20CRv2 (141 winters), **b** the ERA-20C (110 winters) and **c** the NCEP/NCAR-R1 (67 winters) during all winters. The correlations are shown only for the land. Areas with significance at the $p < 0.05$ level are stippled

phase of the PNA in response to the eruptions during the first post-eruption winter. During the second post-eruption winter, the anomaly maps show a pattern largely opposite to the first post-eruption winter over the North Pacific and North America regions (Fig. 7b, d, f). The weaker and insignificant anomalies over the four centers mentioned above suggest a tendency towards a slightly negative PNA. This further indicates that a robust and positive PNA response to strong eruptions only occurs during the first post-eruption winter, which contributes to significant winter warming over northwestern North America (Fig. 3a, c, e). An opposite but insignificant response tends to occur during the second post-eruption winter.

4.4 Superposed epoch analysis

As we showed above, although the composite anomalies suggest a positive PNA-like circulation pattern during the first post-eruption winter, the signal is relatively weak, given small significance areas in the PNA-relevant regions (e.g., the Aleutian Islands) (Figs. 5, 7). This implies that individual eruptions can produce a circulation pattern different from the positive PNA for the first post-eruption winter. To access the relative importance of individual eruptions to the PNA, we explore the evolution of winter surface temperature and PNA index for each eruption based on the 20CRv2 dataset (Fig. 9). It is clear that the positive PNA signal for the first post-eruption winter largely derives from recent three eruptions, especially El Chichón and Pinatubo, which have more weight (Fig. 9d, e, f). In contrast, Krakatau, Santa Maria and Novarupta eruptions correspond to slightly positive or even negative temperature (or PNA) anomalies (Fig. 9a, b, c), weakening the positive PNA signal during the first post-eruption winter. Thus, although the positive PNA signal is significant for the first post-eruption winter, it is quite noisy and dominated by the recent three eruptions.

To reduce the noise level, we perform a superposed epoch analysis on the surface temperature anomalies (ΔT) and PNA indices defined in Fig. 1 to assess the robustness of the PNA response to strong volcanic eruptions (Fig. 10). The SEA shows a significant ($p < 0.01$) peak in temperature anomalies (>1.8 K) over northwestern North America during the first post-eruption winter, though the amplitudes are dependent on the cases of eruptions (Fig. 10a). These positive temperature anomalies originate from enhanced heat advection that results from a significant ($p < 0.05$) positive phase of the PNA (PNA index >1.7 for all three reanalyses) during the first post-eruption winter (Fig. 10b). The second post-eruption winter, however, is characterized by slightly negative and insignificant anomalies (<−0.2 K) over northwestern North America, which are consistent with low (0.6 for the ERA-20C) and even negative PNA indices (−0.3 and −0.8 for the 20CRv2 and the NCEP/NCAR R1, respectively).

The climate response to volcanic eruptions is sensitive to the choice of volcanoes (Robock and Mao 1995). Some small eruptions usually have a weak climatic effect because they inject limited volcanic aerosols into the stratosphere (Robock 2000). To further test the robustness of the PNA response to volcanic forcing, we repeat the superposed epoch analysis by including some small eruptions that were examined previously (Christiansen 2008). This does not make much difference to our results (Fig. S1). Adding the five relatively small eruptions to existing six appears to slightly weaken the robustness of the positive PNA signal for the first post-eruption winter, but it is still significant at the 0.05 or 0.1 confidence level.

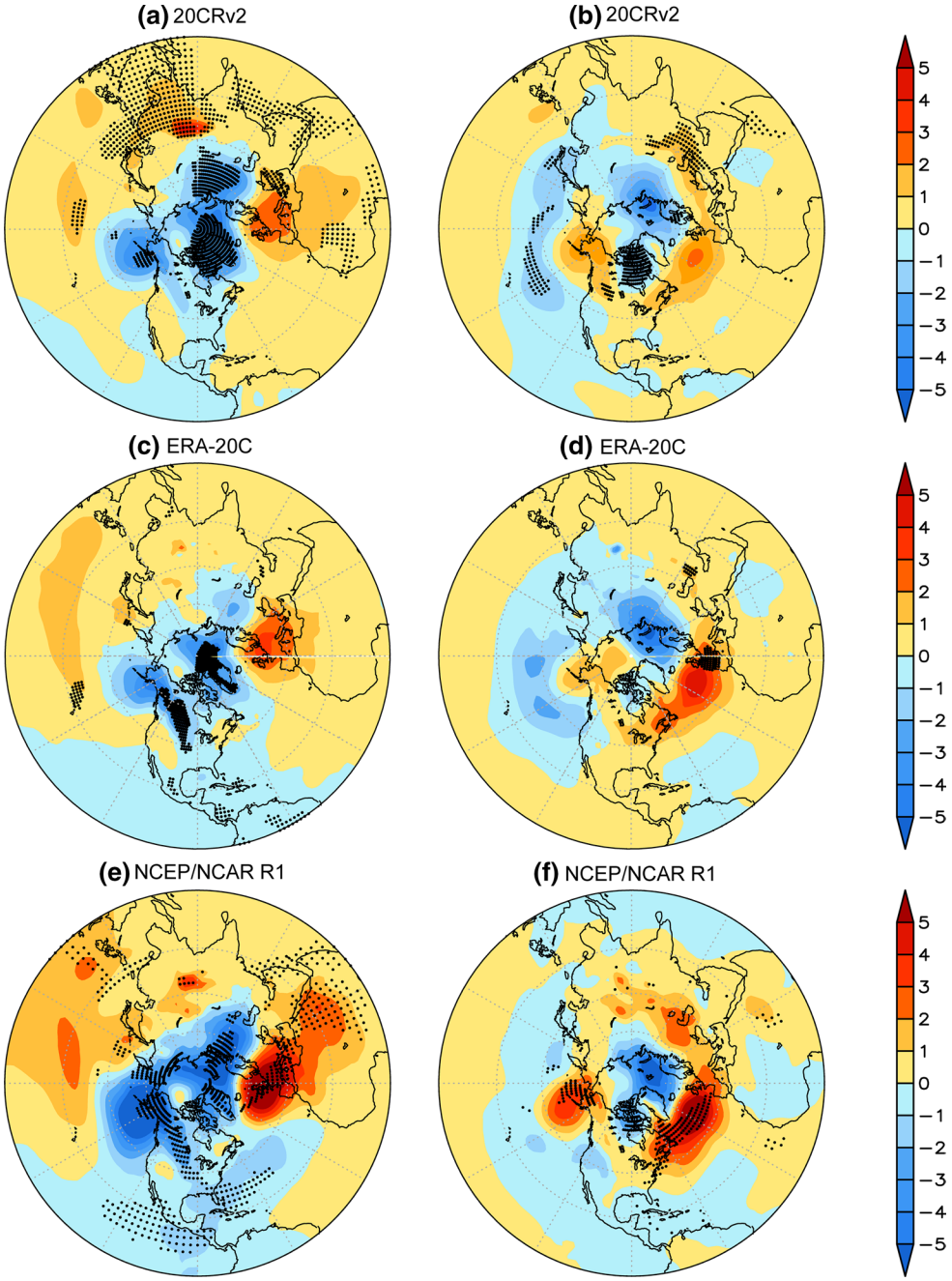

Fig. 5 Composite anomalies of the MSLP (hPa) for the first (*left*) and second (*right*) winters following the eruptions based on the 20CRv2, the ERA-20C and the NCEP/NCAR R1, respectively. Areas with significance at the $p < 0.05$ level are stippled

The SEA further corroborates that the PNA tends to be more positive in response to strong volcanic eruptions during the first post-eruption winter. An insignificant PNA signal during the second post-eruption winter is an unexpected result relative to previous studies that indicate a positive temperature anomaly over northwestern North America (Robock and Mao 1992, 1995; Shindell and Schmidt 2004 2004). However, a recent study has also demonstrated an insignificant PNA response to strong eruptions during the second post-eruption winter (Christiansen 2008), though the reason for this response is still not clear.

4.5 Possible ENSO modulation of the volcanic influence

To identify whether there is an influence of ENSO on the PNA response to strong eruptions, we examine the climate anomalies with ENSO signal removed. The results show that there are no remarkable changes in spatial patterns of winter surface temperature and geopotential height anomalies by removing the ENSO signal (Figs. S2, S3), compared with those including ENSO signal (Figs. 3, 7). The positive PNA-like signals during the first post-eruption winter still remain robust, though the anomalies slightly weaken in magnitude.

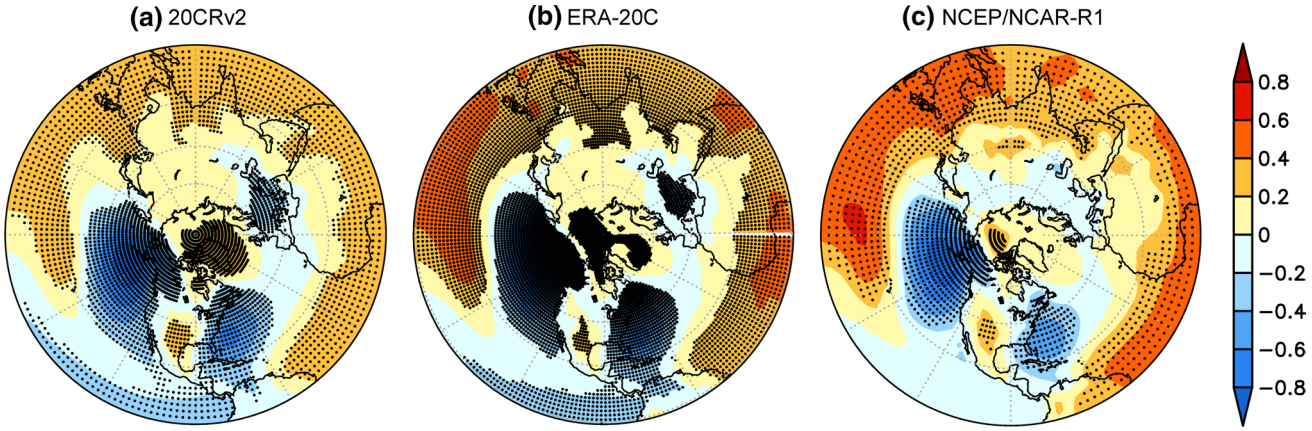

Fig. 6 Spatial correlations between the MSLP and the PNA index for **a** the 20CRv2 (141 winters), **b** the ERA-20C (110 winters) and **c** the NCEP/NCAR-R1 (67 winters) during all winters. Areas with significance at the $p < 0.05$ level are stippled

The SEA provides a clearer assessment of the ENSO modulation of the volcanic influence on the PNA (Fig. 10c, d). When the ENSO signal is linearly removed, the mean surface temperature anomaly in northwestern North America slightly decreases in magnitude and significance, but a positive PNA signal is still robust for the first post-eruption winter (Fig. 10c). This also largely holds true for the PNA index. Though the mean PNA index (1.3) for the 20CRv2 is still significantly positive at the 0.01 confidence level, the ERA-20C (PNA index = 1.0, $p < 0.1$) and the NCEP/NCAR R1 (PNA index = 1.5, $p < 0.05$) datasets show a less robust response (Fig. 10d). These results suggest that the PNA tends to be in the positive phase during the first post-eruption winter, but both the magnitude and significance depend partly on the modulation of ENSO variability.

5 Discussion

5.1 Possible mechanisms for the PNA response to strong volcanic eruptions

Although strong volcanic eruptions tend to force a positive phase of the PNA during the first post-eruption winters, the physical links between the volcanic eruptions and PNA is still not well known. Previous studies indicated that the response of winter tropospheric circulation to strong volcanic eruptions can be plausibly explained by a dynamical coupling of the tropospheric circulation to the state of the stratospheric polar vortex (Kodera 1994; Stenchikov et al. 2002). They argued that after a large eruption, the volcanic aerosols injected into the stratosphere can heat the tropical lower stratosphere by absorption of near-infrared radiation, which leads to an increase in the equator-to-pole temperature gradient. This in turn leads to a strong stratospheric polar vortex. The strengthening of the polar vortex modulates the planetary wave field in such a way that an anomalously positive PNA pattern is produced in the troposphere over the Pacific and North American sectors (Perlwitz and Graf 1995).

Figure 11 shows the composite anomalies of the 50-hPa geopotential height and Pacific SST (Smith et al. 2008) during the two winters after the eruptions. For the first post-eruption winter, the 50-hPa geopotential height anomalies reveal a significant ($p < 0.05$) strong stratospheric polar vortex (Fig. 11a), with strong negative anomalies at high latitudes and positive anomalies at tropical and sub-tropical latitudes. This strong meridional geopotential height gradient leads to enhanced westerly winds at the edge of the polar vortex, which can penetrate into the troposphere and interact with the topography leading changes in phase and amplitude of mid-latitude tropospheric planetary waves (Castanheira et al. 2009) and producing a pattern of the positive PNA in the Pacific and North American sectors (Kodera 1994). This explanation is consistent with the statistical findings reported by Perlwitz and Graf (1995) who identified that increased planetary wave-number one in the stratosphere can produce a barotropic mode resembling a positive PNA in the troposphere. However, the second post-eruption winter, though it also projects a significant strong polar stratospheric vortex, reveals a weak equator-to-pole geopotential height gradient (Fig. 11b). The resulting weak westerly winds may limit downward propagation of planetary waves from the stratosphere to the troposphere during the second post-eruption winter. In addition to the above mechanism, previous modeling studies suggested that the imposed SSTs can modulate the stratosphere-troposphere interaction (Kirchner et al. 1999; Stenchikov et al. 2002). The tropical SSTs typically decrease during the first three winters after a strong eruption because of aerosol radiative

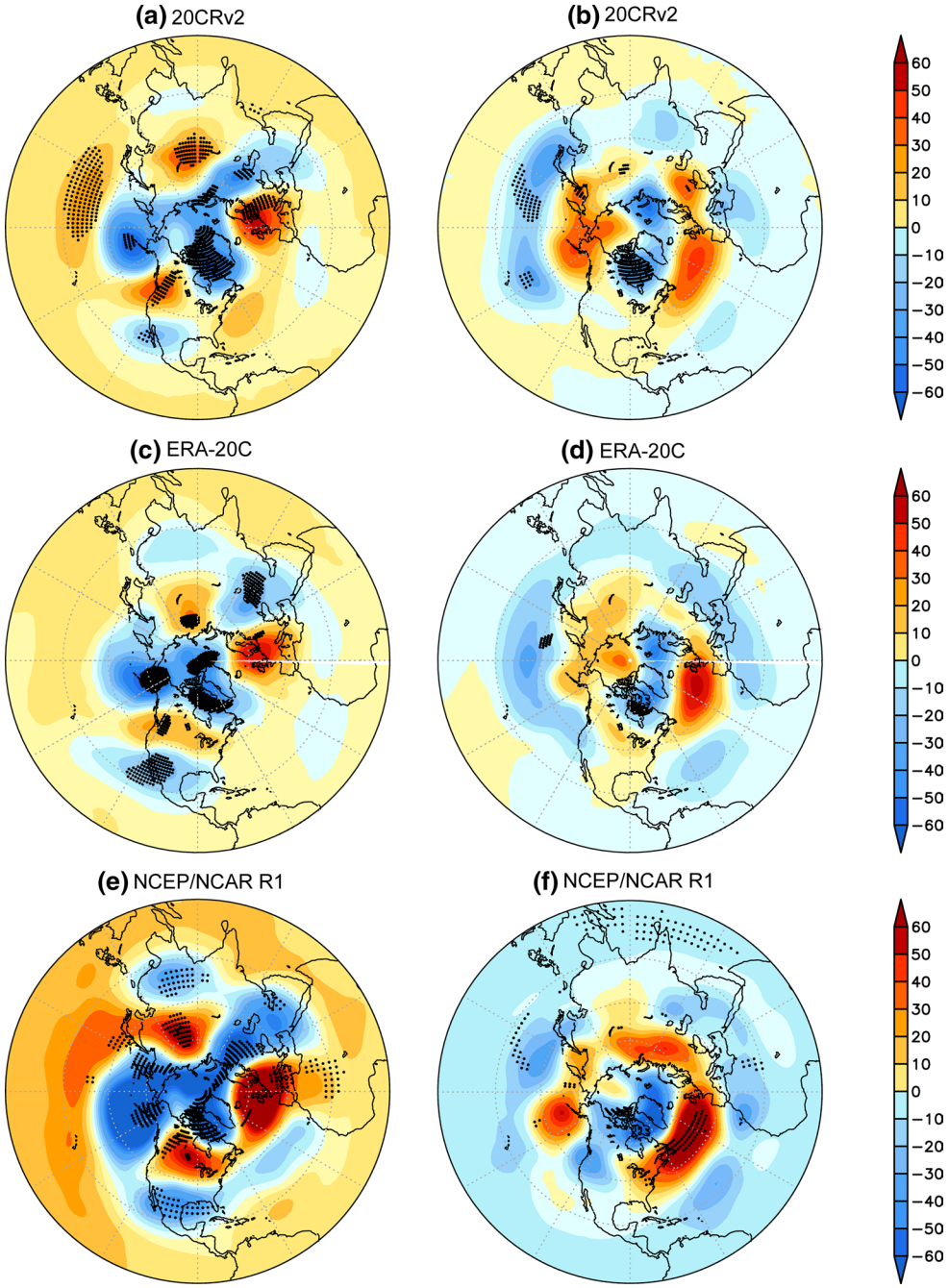

Fig. 7 Composite anomalies of the 500-hPa geopotential height (m) for the first (*left*) and second (*right*) winters following the eruptions based on the 20CRv2, the ERA-20C and the NCEP/NCAR R1, respectively. Areas with significance at the $p < 0.05$ level are stippled

cooling (Zanchettin et al. 2012, 2013). Our analysis shows a significant ($p < 0.05$) positive SST anomaly (El Niño-like pattern) in the central and eastern tropical Pacific for the first post-eruption winter (Fig. 11c), with a slight negative but insignificant anomaly (La Niña-like pattern) in the region for the second post-eruption winter (Fig. 11d). This El Niño-like pattern during the first post-eruption winter may further enhance the positive PNA signal (Perlwitz and Graf 1995; Graf et al. 2014). Instead, the slight La Niña-like pattern in the central and eastern tropical Pacific for the second post-eruption winter may contribute to negative PNA signal.

Our study suggests that the warming effect of strong volcanic eruption in northwestern North American continent due to the positive PNA circulation is more consistent with previous studies (Robock 2000, and references therein) for the first post-eruption winter, but the weak (even slight cooling) signal in this region for the second post-eruption winter seems unexpected. Robock and Mao (1992) found that the winter warming in the Northern Hemisphere

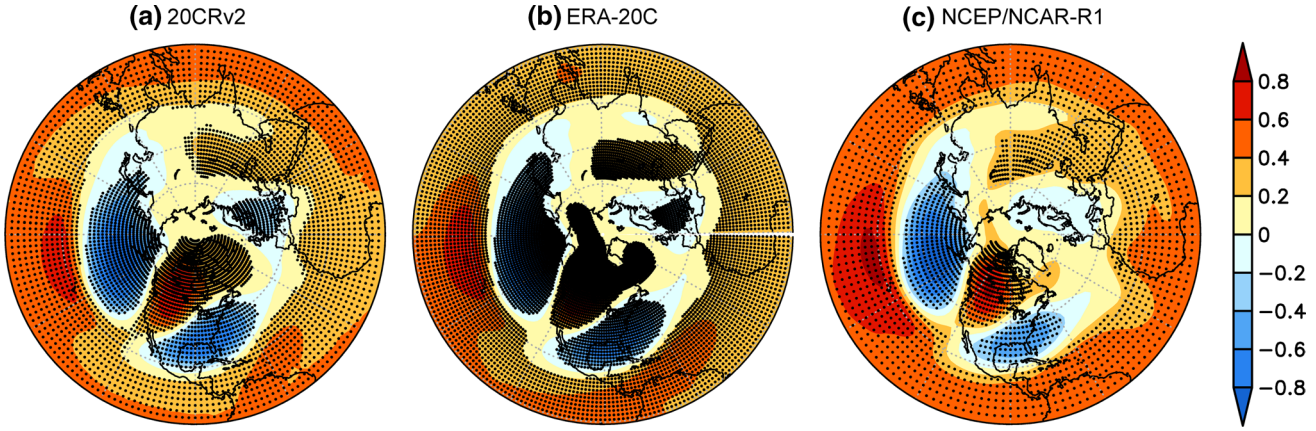

Fig. 8 Spatial correlations between the 500-hPa geopotential height and the PNA index for **a** the 20CRv2 (141 winters), **b** the ERA-20C (110 winters) and **c** the NCEP/NCAR-R1 (67 winters) during all winters. Areas with significance at the $p < 0.05$ level are stippled

occurred in the first winter after strong tropical eruptions, but in the second winter only for strong extratropical eruptions. The major eruptions selected in this study include six volcanoes, of which only one (Novarupta) is in the extratropics with lowest AOD, and the others are located in the tropics (Table 1; Fig. 1a). Thus, the weak (even slightly negative PNA) signal during the second winters after the eruptions may reflect some bias in selection of volcanic events.

The dynamical mechanisms for the response of climate to strong volcanic eruption are complex and still remain some uncertainty, particularly regarding the wave propagation through the polar stratosphere (Graf et al. 2007). Though we present a simple discussion about the physical link between the PNA and volcanic eruptions, the associated mechanisms still need to be understood and future work should involve modeling experiments to further investigate the dynamical response of the PNA to volcanic forcing.

5.2 Implications for North American climate studies

The results presented in this study represent a necessary step forward toward a more complete evaluation of the PNA response to strong volcanic eruptions, though there still remains some uncertainty due to relatively low-quality data before 1950. A framework for understanding the influence of strong volcanic eruption on the PNA has some implications for the detection and attribution of modern and past climatic changes in North America. Previous studies have suggested that there is a significant warming over western North America, but a slight cooling over eastern North America in the first and/or second winter after the volcanic eruptions as summarized by Robock (2000). This volcanic signal is also robust for North American winter precipitation, with drier conditions across the Pacific Northwest, Northern Rocky Mountains and upper Midwestern United States, and wetter conditions in the southwestern and southeastern United States and across the central and southern Great Plains during the two winter following the eruptions (Iles et al. 2013; Iles and Hegerl 2014). These spatial patterns in temperature and precipitation are generally consistent with those associated with a positive phase of the PNA (Leathers et al. 1991). Based on our present findings, we suggest that volcanic eruptions may affect North American surface climates via the modulation of the PNA. Recently discovered robust PNA signals in isotopes of modern precipitation (Birks and Edwards 2009; Liu et al. 2011, 2012, 2014c) and paleo-proxies (Moore et al. 2002; Trouet and Taylor 2010; Liu et al. 2014a) have suggested that the PNA influences hydroclimate variability across North America by modulating midtropospheric atmospheric circulation patterns and storm tracks. Thus, an improved understanding of the PNA/volcanoes relationship will represent a step toward in constraining the role of strong volcanic eruptions on modern and past changes in circulation, temperature and precipitation across North America. For example, some evidence (Crowley and North 1991) suggests that a more meridional flow across North America is associated with the positive PNA during the Little Ice Age (LIA). Given our present findings, such a circulation feature may be consistent with the response to the general increase in volcanic eruptions during the LIA and lower solar activity (Crowley 2000), which can also induce a positive PNA circulation pattern (Trouet and Taylor 2010; Liu et al. 2014b).

6 Conclusions

The present study is in many ways a continuation of the discussion about volcanic influence on PNA brought up by Christiansen (2008), aiming at providing a more rigorous

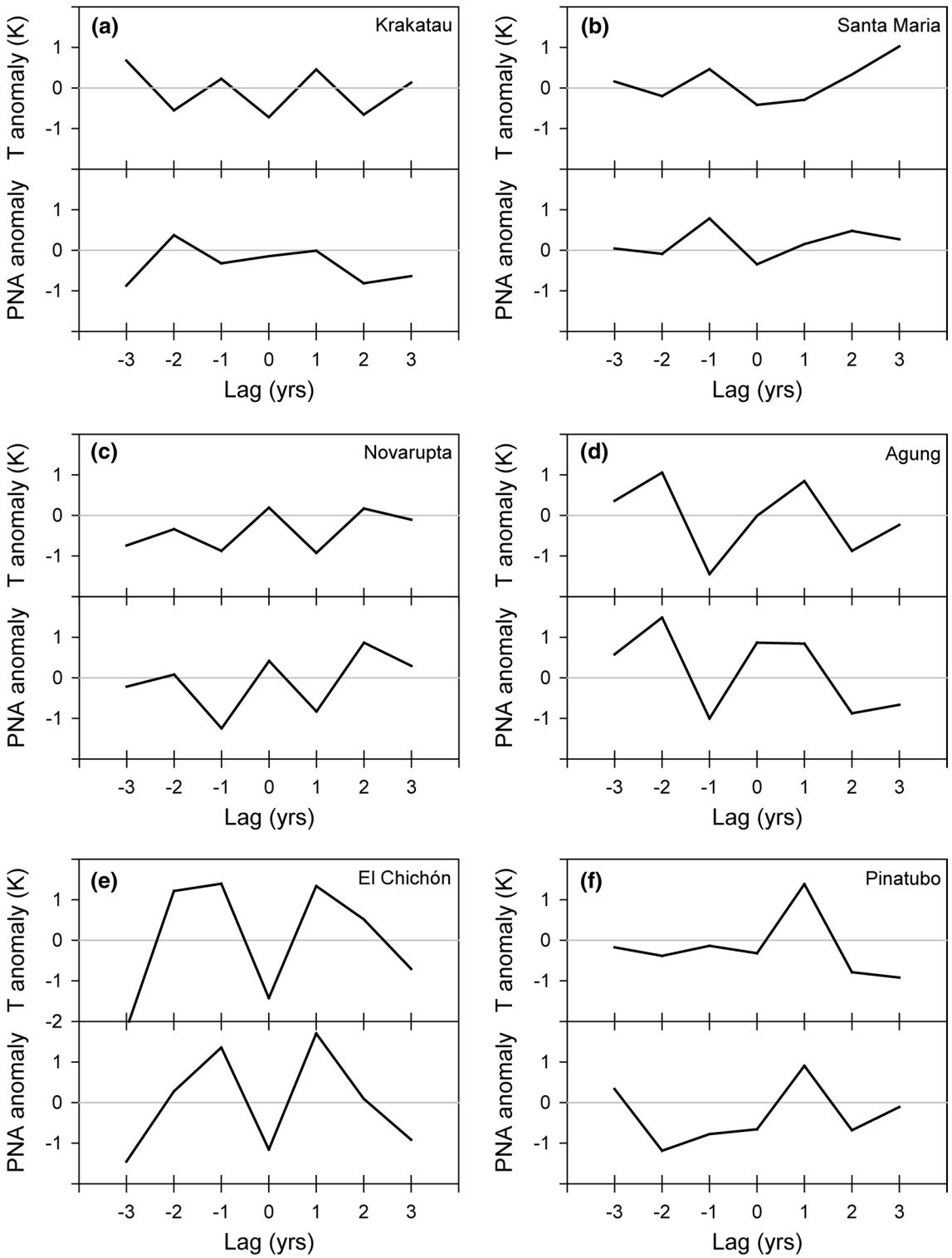

Fig. 9 Response of winter surface temperature and PNA to each volcanic eruption. The surface temperature and PNA index are as defined in Fig. 1, but the anomalies are calculated with respect to the means for the reference periods listed in Table 1

test of how the largest volcanic eruptions affect the PNA pattern. We used three different reanalysis datasets to investigate the changes in the PNA during the first and second winters following six strong volcanic eruptions. We found a significant warming over northwestern North America during the first post-eruption winter, with a slight but insignificant cooling during the second post-eruption winter. Analyses of composite anomalies of the MSLP and 500-hPa

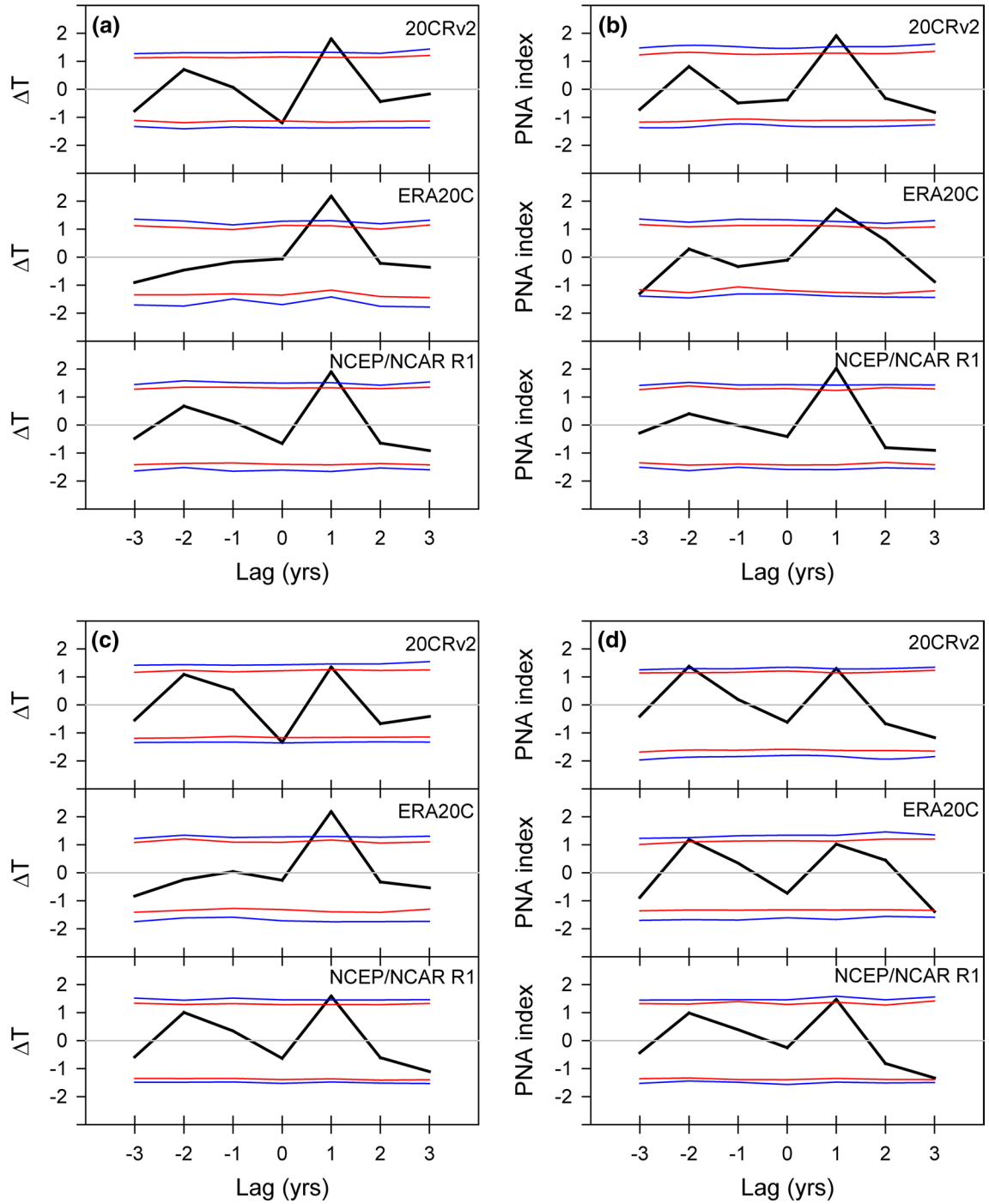

Fig. 10 Superposed epoch analysis of the winter means of the surface temperature anomaly (K) (*left*) and PNA index (*right*) defined in Fig. 1 before (*top*) and after (*bottom*) removing ENSO signal based on the 20CRv2, the ERA-20C and the NCEP/NCAR R1, respectively. The average over different volcanic eruptions is shown at different lag time. *Lag 1* indicates the first winter after the eruptions. The *red* and *blue lines* show the confidence intervals of 5–95 % and 1–99 % derived from 1000 Monte Carlo simulations, respectively

geopotential height fields indicated that this warming over northwestern North America is associated with a positive phase of the PNA. It is expressed by slightly intensified high pressure anomalies over the subtropical Pacific and northwestern North America, and low pressure anomalies around the Aleutian Islands and southern United States. Although these anomalies are relatively weak and represent very small significant areas in the PNA-relevant regions due to some noise, they lead to a positive PNA-like circulation pattern, driving enhanced southwesterly flows to northwestern

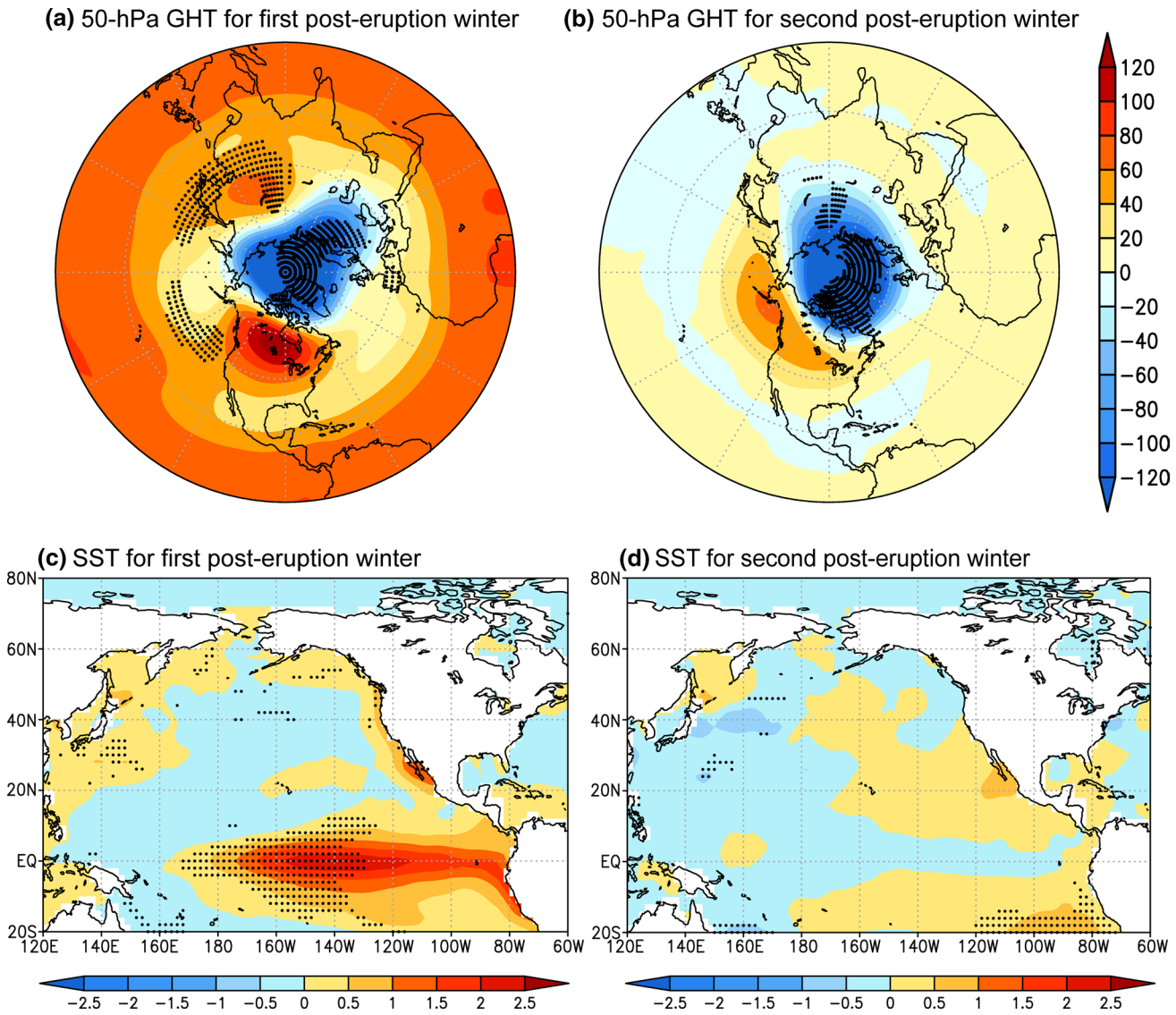

Fig. 11 Composite anomalies of the 50-hPa geopotential height (m) (*top*) and Pacific SST (°C) (*bottom*) for the first (*left*) and second (*right*) winters following the eruptions based on recent three eruptions. Areas with significance at the $p < 0.05$ level are stippled

North America resulting in a significant warming in the region. In contrast, the second post-eruption winter does not show a robust PNA response to the eruptions. These findings agree with Christiansen (2008). We further found that the response of the PNA to strong eruptions depends partly on the phase of the ENSO. When the ENSO influence is linearly removed, the PNA still favors a significant positive pattern during the first post-eruption winter, albeit with decreased magnitude and significance. Our results further corroborate the findings of Christiansen (2008), but are entirely independent of his analyses confined to the historical MSLP data. Thus, our analysis provides new evidence of a link between the PNA and volcanic eruptions. Nevertheless, the robustness of the results and associated physical mechanisms governing the PNA response to volcanic eruptions warrant further careful study.

Acknowledgments We are grateful to Dr. Olivier Blarquez for his help with the superposed epoch analysis, Dong Chen and Haimao Lan for assistance with data processing. We also thank the editor and anonymous reviewers for their insightful comments that have greatly improved the quality of the paper. This work was supported by the China Young 1000-Talent Program and the National Science Foundation of China Grants (41305131).

References

Adams JB, Mann ME, Ammann CM (2003) Proxy evidence for an El Nino-like response to volcanic forcing. Nature 426:274–278

Birks SJ, Edwards TWD (2009) Atmospheric circulation controls on precipitation isotope–climate relations in western Canada. Tellus B 61:566–576

Briffa KR, Jones PD, Schweingruber FH, Osborn TJ (1998) Influence of volcanic eruptions on Northern Hemisphere summer temperature over the past 600 years. Nature 393:450–455

Castanheira J, Liberato M, De La Torre L, Graf H, DaCamara C (2009) Baroclinic Rossby wave forcing and barotropic Rossby wave response to stratospheric vortex variability. J Atmos Sci 66:902–914

Charlton-Perez AJ, Baldwin MP, Birner T, Black RX, Butler AH, Calvo N, Davis NA, Gerber EP, Gillett N, Hardiman S (2013) On the lack of stratospheric dynamical variability in low-top versions of the CMIP5 models. J Geophys Res 118:2494–2505

Christiansen B (2008) Volcanic eruptions, large-scale modes in the Northern Hemisphere, and the El Niño-Southern Oscillation. J Clim 21:910–922

Compo GP, Sardeshmukh PD (2010) Removing ENSO-related variations from the climate record. J Clim 23:1957–1978

Compo GP, Whitaker JS, Sardeshmukh PD, Matsui N, Allan RJ, Yin X, Gleason BE, Vose R, Rutledge G, Bessemoulin P (2011) The twentieth century reanalysis project. Q J R Meteorol Soc 137:1–28

CPC (2016) Teleconnections: Pacific/North American pattern: monthly mean PNA index. National Weather Service Climate Prediction Center. Accessed 1 Jan 2016. www.cpc.ncep.noaa.gov/products/precip/CWlink/pna/month_pna_index2.shtml

Crowley JW (2000) Causes of climate change over the past 1000 years. Science 289:270–277

Crowley TJ, North GR (1991) Paleoclimatology. Oxford University Press, New York, p 349

Deser C, Wallace J (1987) El Nino events and their relation to the Southern Oscillation: 1925–1986. J Geophys Res 92:14189–14196

Driscoll S, Bozzo A, Gray LJ, Robock A, Stenchikov G (2012) Coupled Model Intercomparison Project 5 (CMIP5) simulations of climate following volcanic eruptions. J Geophys Res 117:D17105. doi:10.1029/2012JD017607

Esper J, Schneider L, Krusic PJ, Luterbacher J, Büntgen U, Timonen M, Sirocko F, Zorita E (2013) European summer temperature response to annually dated volcanic eruptions over the past nine centuries. Bull Volcanol 75:1–14

Fischer E, Luterbacher J, Zorita E, Tett SFB, Casty C, Wanner H (2007) European climate response to tropical volcanic eruptions over the last half millennium. Geophys Res Lett 34:L05707. doi:10.1029/2006GL027992

Graf H-F, Li Q, Giorgetta M (2007) Volcanic effects on climate: revisiting the mechanisms. Atmos Chem Phys 7:4503–4511

Graf H-F, Zanchettin D, Timmreck C, Bittner M (2014) Observational constraints on the tropospheric and near-surface winter signature of the Northern Hemisphere stratospheric polar vortex. Clim Dyn 43:3245–3266

Iles CE, Hegerl GC (2014) The global precipitation response to volcanic eruptions in the CMIP5 models. Environ Sci Lett 9:104012

Iles CE, Hegerl GC, Schurer AP, Zhang X (2013) The effect of volcanic eruptions on global precipitation. J Geophys Res 118:8770–8786

Kalnay EC, Kanamitsu M, Kistler R, Collins W, Deaven D, Gandin L, Iredell M, Saha S, White G, Woollen J (1996) The NCEP/NCAR 40-year reanalysis project. Bull Am Meteorol Soc 77:437–471

Kirchner I, Stenchikov GL, Graf HF, Robock A, Antuña JC (1999) Climate model simulation of winter warming and summer cooling following the 1991 Mount Pinatubo volcanic eruption. J Geophys Res 104:19039–19055

Kodera K (1994) Influence of volcanic eruptions on the troposphere through stratospheric dynamical processes in the Northern Hemisphere winter. J Geophys Res 99:1273–1282

L'Heureux ML, Lee S, Lyon B (2013) Recent multidecadal strengthening of the Walker circulation across the tropical Pacific. Nat Clim Change 3:571–576

Larson SM, Kirtman BP (2014) The Pacific meridional mode as an ENSO precursor and predictor in the North American multimodel ensemble. J Clim 27:7018–7032

Leathers DJ, Yarnal B, Palecki MA (1991) The Pacific/North American teleconnection pattern and United States climate. Part I: regional temperature and precipitation associations. J Clim 4:517–528

Liu Z, Kennedy CD, Bowen GJ (2011) Pacific/North American teleconnection controls on precipitation isotope ratios across the contiguous United States. Earth Planet Sci Lett 310:319–326

Liu Z, Bowen GJ, Welker JM, Yoshimura K (2012) Winter precipitation isotope slopes of the contiguous USA and their relationship to the Pacific/North American (PNA) pattern. Clim Dyn 41:403–420

Liu Z, Yoshimura K, Bowen GJ, Buenning NH, Risi C, Welker JM, Yuan F (2014a) Paired oxygen isotope records reveal modern North American atmospheric dynamics during the Holocene. Nat Commun 5:3701. doi: 10.1038/ncomms4701

Liu Z, Yoshimura K, Buenning NH, He X (2014b) Solar cycle modulation of the Pacific-North American teleconnection influence on North American winter climate. Environ Res Lett 9:024004

Liu Z, Yoshmura K, Bowen GJ, Welker JM (2014c) Pacific North American teleconnection controls on precipitation isotopes ($\delta^{18}O$) across the contiguous United States and adjacent regions: a GCM-based Analysis. J Clim 27:1046–1061

Maher N, McGregor S, England MH, Gupta AS (2015) Effects of volcanism on tropical variability. Geophys Res Lett 42:6024–6033

Mann ME, Fuentes JD, Rutherford S (2012) Underestimation of volcanic cooling in tree-ring-based reconstructions of hemispheric temperatures. Nat Geosci 5:202–205

Mao J, Robock A (1998) Surface air temperature simulations by AMIP general circulation models: volcanic and ENSO signals and systematic errors. J Clim 11:1538–1552

Mitchell JM (1961) Recent secular changes of global temperature. Ann NY Acad Sci 95:235–250

Moore G, Holdsworth G, Alverson K (2002) Climate change in the North Pacific region over the past three centuries. Nature 420:401–403

Perlwitz J, Graf H-F (1995) The statistical connection between tropospheric and stratospheric circulation of the Northern Hemisphere in winter. J Clim 8:2281–2295

Poli P, Hersbach H, Tan D, Dee D, Thepaut J-N, Simmons A, Peubey C, Laloyaux P, Komori T, Berrisford P (2013) The data assimilation system and initial performance evaluation of the ECMWF pilot reanalysis of the 20th-century assimilating surface observations only (ERA-20C). Technical report, ERA report series 14

Renwick JA, Wallace JM (1996) Relationships between North Pacific wintertime blocking, El Niño, and the PNA pattern. Mon Weather Rev 124:2071–2076

Robock A (2000) Volcanic eruptions and climate. Rev Geophys 38:191–219

Robock A, Mao J (1992) Winter warming from large volcanic eruptions. Geophys Res Lett 19:2405–2408

Robock A, Mao J (1995) The volcanic signal in surface temperature observations. J Clim 8:1086–1103

Robock A, Adams T, Moore M, Oman L, Stenchikov G (2007) Southern Hemisphere atmospheric circulation effects of the 1991 Mount Pinatubo eruption. Geophys Res Lett 34:L23710. doi:10.1029/2007GL031403

Sato M, Hansen JE, McCormick MP, Pollack JB (1993) Stratospheric aerosol optical depths, 1850–1990. J Geophys Res 98:22987–22994

Shindell DT, Schmidt GA (2004) Southern Hemisphere climate response to ozone changes and greenhouse gas increases. Geophys Res Lett 31:L18209. doi:10.1029/2004GL020724

Smith TM, Reynolds RW, Peterson TC, Lawrimore J (2008) Improvements to NOAA's historical merged land–ocean surface temperature analysis (1880–2006). J Clim 21:2283–2296

Stenchikov G, Robock A, Ramaswamy V, Schwarzkopf MD, Hamilton K, Ramachandran S (2002) Arctic Oscillation response to the 1991 Mount Pinatubo eruption: effects of volcanic aerosols and ozone depletion. J Geophys Res 107(D24):4803. doi:10.1029/2002JD002090

Stenchikov G, Hamilton K, Stouffer RJ, Robock A, Ramaswamy V, Santer B, Graf HF (2006) Arctic Oscillation response to volcanic eruptions in the IPCC AR4 climate models. J Geophys Res 111:D07107. doi:10.1029/2005JD006286

Timmreck C (2012) Modeling the climatic effects of large explosive volcanic eruptions. Wiley Interdiscip Rev Clim Change 3:545–564

Trouet V, Taylor AH (2010) Multi-century variability in the Pacific North American circulation pattern reconstructed from tree rings. Clim Dyn 35:953–963

Wallace JM, Gutzler DS (1981) Teleconnections in the geopotential height field during the Northern Hemisphere winter. Mon Weather Rev 109:784–812

Yu B, Shabbar A, Zwiers F (2007) The enhanced PNA-like climate response to Pacific interannual and decadal variability. J Clim 20:5285–5300

Zanchettin D, Timmreck C, Graf H-F, Rubino A, Lorenz S, Lohmann K, Krüger K, Jungclaus J (2012) Bi-decadal variability excited in the coupled ocean–atmosphere system by strong tropical volcanic eruptions. Clim Dyn 39:419–444

Zanchettin D, Bothe O, Graf HF, Lorenz SJ, Luterbacher J, Timmreck C, Jungclaus JH (2013) Background conditions influence the decadal climate response to strong volcanic eruptions. J Geophys Res 118:4090–4106